

Structural characteristics and reactivity properties of the tantalum modified mesoporous silicalite (MCM-41) catalysts

Jih-Mirn Jehng^{a,*}, Wan-Chen Tung^a, Chao-His Huang^a, Israel E. Wachs^b

^a Department of Chemical Engineering, National Chung Hsing University, 250 Kuokuang Road, Taichung 402, Taiwan, ROC

^b Department of Chemical Engineering, Lehigh University, 7 Asa Drive, Bethlehem, PA 18015, USA

Received 2 June 2006; received in revised form 31 August 2006; accepted 25 September 2006

Available online 13 November 2006

Abstract

The structural characteristics of the Ta–MCM-41 catalyst have been investigated by BET measurement, small angle X-ray diffraction, UV–vis–NIR diffuse reflectance spectroscopy (DRS) and Raman spectroscopy techniques. Three types of tantalum oxide species: an isolated TaO₄ species in the MCM-41 framework, an isolated surface TaO₄ species on the MCM-41 surface, and bulk Ta₂O₅, can be present individually or coexist on the Ta–MCM-41 catalysts, and its relatively intensity is dependent on the Ta concentration. The local structure of the Ta atoms in the Ta–MCM-41 catalyst forms an isolated active site with the bridging Ta–O–Si bonds on the surface and in the frame structure of MCM-41. The catalytic properties of the Ta–MCM-41 catalysts were chemically probed with propane oxidative dehydrogenation (ODH) and methanol oxidation reactions in order to distinguish the different surface active sites present on the catalyst. Consequently, the well-dispersed isolated active sites exhibit high redox catalytic properties to produce formaldehyde (HCHO) and methyl formate (MF), and bulk Ta₂O₅ only possesses acid sites to form dimethyl ether (DME). The presence of Ta–O–Si bonds in the catalyst is responsible for the high reactivity/selectivity of the oxidation reactions.

© 2006 Elsevier Inc. All rights reserved.

Keywords: Mesoporous material; Fourier transform infrared spectroscopy; Raman spectroscopy; Propane oxidative dehydrogenation; Methanol oxidation

1. Introduction

M41S has been newly discovered as a mesoporous material by Beck et al. [1]. MCM-41, a member of M41S family, contains a hexagonal array of tubular pores possessing a high surface area and uniform pore size. It was synthesized with a self-assembly mechanism for the silicate source and surfactants with a long chain length as the template, and the structure of MCM-41 can be incorporated with a metal atom to substitute Si⁴⁺ atom in the framework. The substitution of Si with the transition metals in MCM-41 has been reported in many literatures such as V [2–8], Nb [9–12], W [13–15], Mo [14,16,17], V–Mo [18], Cr [19–22], Ti [23–26],

and Zr [26] for selective oxidation of hydrocarbons, liquid-phase oxidation using H₂O₂, polymerization, and photocatalysis applications. It appears that the local structure of the metal atoms in the M–MCM-41 can present as an isolated active site with similar bridging M–O–Si bonds on the surface and in the frame structure of MCM-41 [2,4,7,10–12,27–29]. The dispersed and isolated active sites exhibit high catalytic properties and the bridging M–O–Si bonds are the critical functionalities for catalytic applications.

The formation of the bridging M–O–Si bonds has also reported on silica-supported metal oxide catalysts which show high selectivity to oxygenate and olefins for the oxidative dehydrogenation (ODH) of short chain paraffins [30–35]. The surface vanadia species supported on silica are well-known to possess an isolated and distorted VO₄ structure with a single V=O terminal bond and three

* Corresponding author. Tel.: +886 4 22852439; fax: 886 4 22854734.

E-mail addresses: jmjehng@dragon.nchu.edu.tw (J.-M. Jehng), iew0@lehigh.edu (I.E. Wachs).

V–O–Si bridging bonds anchored on silica support [36–41]. The distorted V^{5+} species with the bridging V–O–Si can be found in different silica environments (silica-supported, silicalite, and cogel) and possess similar reducibility and catalytic properties for methanol oxidation [7]. Similar studies on the surface Nb^{5+} species present in both Nb–MCM-41 and Nb_2O_5/SiO_2 catalysts has revealed that the Nb atoms in the Nb–MCM-41 and 1% Nb_2O_5/SiO_2 are predominantly isolated NbO_4 species under dehydration conditions, and surface polymeric niobia species and/or bulk Nb_2O_5 are formed at high niobia loading on silica [11]. The catalytic properties of the dispersed and isolated Nb species in both types of catalysts are active redox sites for methanol oxidation and exhibit similar reactivity and selectivity properties due to the presence of Nb–O–Si bonds in their structure. In recent, the silica-supported tantalum oxide catalyst has been studied to possess isolated TaO_4 species with a surface density about 0.7 Ta atoms/ nm^2 [42]. The catalytic properties of the surface TaO_4 species, which are very different to the bulk Ta_2O_5 with acidic characteristics, have found to possess the redox characteristics due to the presence of the bridging Ta–O–Si bonds on the surface [42]. However, there are no comparative studies on the local structure of the Ta–MCM-41 catalysts with the silica-supported tantalum oxide catalysts to determine the structure–reactivity relationship of the Ta–MCM-41 catalysts.

From the above observations, it is essential to compare the local structure and metal atoms in the MCM-41 structure and on the silica surface in order to understand the molecular structure–reactivity/selectivity relationships of these M–O–Si-based (M = V, Nb, and Ta) catalytic materials. In this study, the incorporation of Ta atom into MCM-41 structure were prepared as a function of the Ta loading, and characterized with BET method to obtain surface area and pore size information; small angle X-ray diffraction (XRD), UV–vis–NIR DRS, and Raman techniques to obtain the structural information. The catalytic properties of the Ta–MCM-41 catalysts were performed with the methanol oxidation and propane ODH reactions, and the combination of the structural information and the catalytic properties can establish the molecular structure–reactivity/selectivity relationship of these catalytic materials.

2. Experimental sections

2.1. Materials and preparations

The Ta–MCM-41 catalyst was prepared by using the $C_{16}TMAB$ (cetyltrimethylammonium bromide, Aldrich) micelles as the template agent, and $TMA Si$ (tetramethylammonium silicate, Aldrich) was used as the silica source. A certain amount of $C_{16}TMAB$ was added to distilled water and stirred to turn into a clear solution (7.8% $C_{16}TMAB$), and mixed with $TMA Si$ with the Si/surfactant ratio equal to 7.5 to form a milky solution. A proper

amount of Ta–Oxalate (Alfa) was added to the mixed solution under the same stirring speed for 2 h at room temperature with various Si/[Ta] molar ratios as 400, 100, 33, 20, and 12 (corresponding to 0.75%, 3%, 8%, 13%, and 20% Ta in MCM-41). The mixture was placed into a Teflon-sealed glass vial, and followed by static heating at 100 °C in the silicon oil bath for 7 days. The white precipitation was then removed, filtered and washed several times with the distilled water. The filtrates was dried for 16 h at room temperature and calcined at 650 °C for 6 h under flowing air to form the Ta–MCM-41 catalyst.

2.2. BET surface area measurements

A volumetric physisorption apparatus (Micromeritics ASAP 2010) was used to determine the BET surface area of the Ta–MCM-41 catalyst. A 0.2–0.5 g of the sample was first degassed with flowing 30 cc/min He gas to remove the impurities and water. Then, the nitrogen gas was introduced into the sample quartz tube to perform the adsorption of nitrogen under the liquid nitrogen temperature. The surface area of the sample was calculated from the amount of adsorbed nitrogen molecules on the surface (based on the N_2 molecule cross-section area is 0.162 nm^2), and the pore size distribution of the catalyst was obtained with BJH (Barrett–Joyner–Halenda) method.

2.3. Small-angle X-ray powder diffraction (small-angle XRD) analysis

The structure and morphology of the Ta–MCM-41 were determined by XRD technique as a function of the composition. The XRD technique was carried out by using the X-ray diffraction instrument (Siemens D5000) using CuK radiation (wave length = 0.154 nm) and the scanning rate was 0.05 deg/min with 2θ from 1 to 10 deg.

2.4. Scanning electron microscopy (SEM)

SEM was used to analyze the morphology of the synthesized Ta–MCM-41 catalysts as a function of Ta concentration. The SEM analysis was carried out using a TOPCON ABT-150S with the energy dispersive spectroscopy operated 10 kV. The sample was evenly spread on the double sticking tape attached to the sample holder, and a thin film of gold was coated on it by using a thin film deposition system to assist the reflection of the electron light.

2.5. UV–vis–NIR diffuse reflectance spectroscopy (DRS)

The DRS experiments were performed on a Varian Gary 5E UV–vis–NIR spectrophotometer. In situ DRS spectra were taken in the range of 200–2200 nm using a Harrick DRS cell (HVC-DR2) to perform the measurements under reaction conditions at elevated temperatures [43,44]. The Harrick cell was slightly modified to accurately measure the temperature around the surface of the catalyst sample

powder. A second thermocouple was added to the sample cup with the probe tip just under the sample surface and close to the spot for spectral recording that is usually around the center of the sample cup. This thermocouple line was not allowed to touch the sample cup, which usually possesses a higher temperature than the catalyst sample [45].

All samples for the in situ measurements were first calcined in the oven at 450 °C for 1 h before immediate transfer to the in situ cell. The sample in the cell was then pretreated at a sample surface temperature of 450 °C in O₂/He for 1 h and cooled down to room temperature. The dehydrated pure MCM-41 was used as the baseline reference for the Ta-MCM-41 catalysts and the MgO was used as the baseline reference for the bulk Ta₂O₅. The DRS spectra were processed with the Bio-Rad Win-IR software, consisting of calculation of the Kubelka-Munk function from the absorbance [46]. A general power law form, suggested by Davis and Mott [47], with $n = 1/2$ for the direct allowed transition ion can be determined by the best linear fit in the lower absorption region was applied to calculate the edge energy (E_g) [48,49].

2.6. Laser Raman spectroscopy

Laser Raman spectroscopic system consists of a quartz cell and a sample holder, a triple-grating spectrometer (Spex, Model 1877), a photodiode array detector (EG&G, Princeton Applied Research, Model 1420), and an argon ion laser (Spectra-Physics, Model 165). The sample holder is made from a metal alloy (Hastalloy C), and a 100–200 mg sample disc is held by the cap of the sample holder. The sample holder is mounted onto a ceramic shaft which can be rotated by a 115 V DC motor at a speed of 1000–2000 rpm, and the Raman spectra were recorded from the region of 400–1200 cm⁻¹.

2.7. Oxidation reactions

The oxidative dehydrogenation (ODH) of propane was carried out in a fixed-bed reactor operating at atmospheric pressure. The reactor has equipped with a coaxial thermocouple to monitor the reaction temperature. A 0.2 g catalyst was placed in an U-shaped quartz reactor using quartz wool to support the sample inside the reactor. The feed gas consists a C₃H₈/O₂ ratio of 1:1, 3:1, and 6:1, respectively, using He gas as a balance gas to maintain the flow rate of 50 cc/min. The reaction temperature were performed from 450 to 550 °C, and the products were analyzed by online gas chromatography (TRE-METRICS 9000 series) equipped with two packed columns of Porapak Q and MS-5A. Porapak Q was used to separate hydrocarbons and CO₂, and MS-5A was used to separate O₂ and CO. The temperature programmed reaction was performed in the following: the oven temperature was first held at 100 °C for 12 min, and then increased with a ramping rate 10 °C/min to 150 °C and maintained for 20 min to separate the final products.

The methanol oxidation reaction was carried out in a fixed-bed differential reactor operating at atmospheric pressure. A mixture of He/O₂ was bubbled through a methanol saturator cooled by a cooler (Neslab RTE110) to obtain a 6/13/81 (mol%) mixture of CH₃OH/O₂/He at a flow rate of ~100 cc/min. The reactor was made of Pyrex glass and held in a vertical position. The 20–70 mg of catalyst was placed at the middle of the reactor between two supporting layers of quartz wool. Before the methanol oxidation reaction, the catalysts were pretreated at 400 °C for 30 min with flowing He/O₂ mixture gas in order to remove adsorbed moisture and any carbonaceous residues. The reaction temperature was performed in the 280–320 °C region, and the outlet of the reactor to the GC was heated to 120–140 °C to avoid condensation of methanol and its products. The reaction products were analyzed by an online GC (HP 5840) equipped with TCD and FID detectors, and two separation columns (Carboxene-1000 packed column and CP-Sil 5CB capillary column).

3. Results

3.1. BET measurements

The nitrogen isotherms of MCM-41 and Ta-MCM-41 catalysts (Fig. 1) follow the type-IV isotherm and show with a sharp capillary condensation step at a relative pressure between 0.2 and 0.4 [9–12] indicating a typical mesoporous structure with uniform pores.

3.2. Small-angle XRD

The XRD patterns of MCM-41 and Ta-MCM-41 catalysts are shown in Fig. 2. The four diffraction peaks (100), (110), (200), and (210) are characteristic of MCM-41 materials possessing a highly ordered hexagonal structure

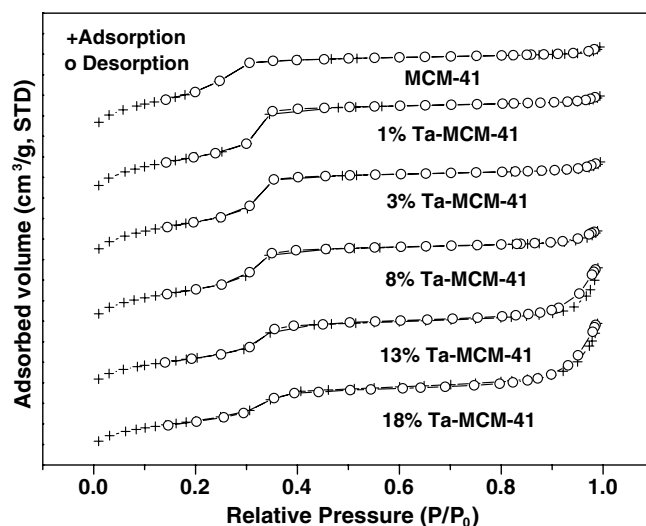


Fig. 1. Nitrogen adsorption/desorption isotherms of the MCM-41 and Ta-MCM-41 catalysts.

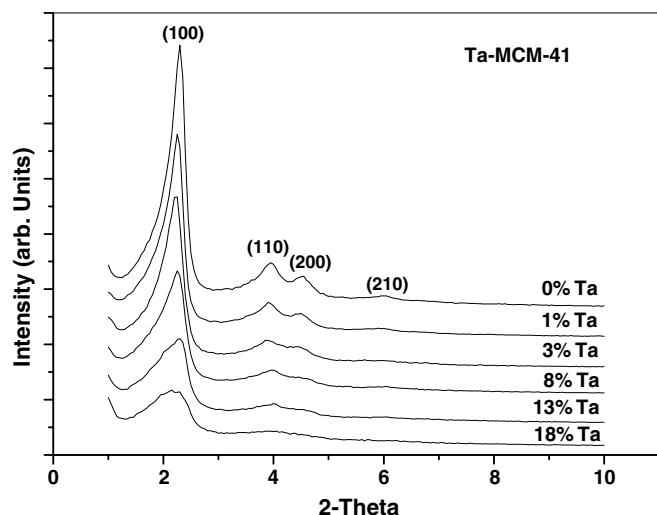


Fig. 2. XRD patterns of the MCM-41 and Ta-MCM-41 catalysts.

[9–12]. The incorporation of Ta atom into the MCM-41 structure results in a slightly shift of (100) toward higher diffraction angle with increasing Ta concentration and the broad and disappearance of the other three smaller diffraction peaks (as shown in Fig. 2).

3.3. Raman studies on the Ta-MCM-41 catalysts

The Raman spectra of the Ta-MCM-41 catalysts are shown in Fig. 3 as a function of Ta concentration. MCM-41 possesses Raman features at 980, ~800, 605, and 490 cm^{-1} , which are very similar to the vibration modes of the silicalite [7] and the amorphous SiO_2 [11]. The 980 cm^{-1} is associated with the Si-OH stretching mode of the surface hydroxyls [7,11]. The bands at 800–830 cm^{-1} and 410–430 cm^{-1} are associated with the symmetric stretching and bending modes of the $[\text{SiO}_4]$ units, however, the broad and weak Raman band at ~1080 cm^{-1} is not so distinguishable due to the anti-symmetric stretching vibration of the tetrahedral $[\text{SiO}_4]$ units [50,51]. The broad bands at ~605 and ~490 cm^{-1} are attributed to tri- and tetra-cyclosiloxane rings, respectively [52,53].

3.4. UV-vis-NIR DRS studies

The edge energies of the Ta-reference compounds, $\text{Ta}_2\text{O}_5/\text{SiO}_2$, and the Ta-MCM-41 catalysts are listed in Table 1. Bulk Ta_2O_5 and MgTa_2O_6 possess a polymerized TaO_6 octahedral structure [42] and a distorted TaO_6 octahedral structure [54,55] exhibiting edge energies below 4.0 eV. The $\text{Ta}_2\text{O}_5/\text{SiO}_2$ and Ta-MCM-41 catalysts exhibit the high edge energy above 4.5 eV.

3.5. Oxidation reactions

The catalytic results of the propane ODH over the Ta-MCM-41 catalysts at 500 °C are presented in Fig. 4 as a

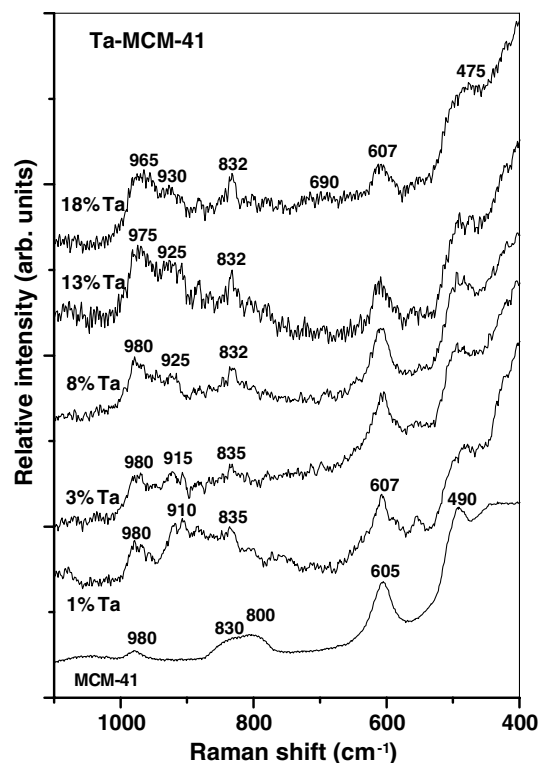


Fig. 3. Raman spectra of the MCM-41 and Ta-MCM-41 catalysts as a function of Ta concentration.

Table 1

Edge energies of Nb-containing oxides/compounds and catalysts

Sample	E_g (eV) (hydrated)	E_g (eV) (dehydrated)	Structural assignments
Ta_2O_5	3.8		Polymerized TaO_6
MgTa_2O_6	4.0		Distorted TaO_6
1% $\text{Ta}_2\text{O}_5/\text{SiO}_2$	–	4.4	Isolated TaO_4
0.25% Ta-MCM-41	–	4.8	Isolated TaO_4
1% Ta_2O_5 -MCM-41	–	4.7	Isolated TaO_4
3% Ta_2O_5 -MCM-41	–	4.5	Isolated TaO_4
8% Ta_2O_5 -MCM-41	–	4.6	Isolated TaO_4

function of Ta concentration and the $\text{C}_3\text{H}_8/\text{O}_2$ ratio. The reactivity of the propane ODH over the Ta-MCM-41 catalyst decreases with increasing Ta concentration up to 3% and remains constant with further increasing Ta concentration. The catalytic properties of the Ta-MCM-41 catalysts were further probed with the sensitive methanol oxidation reaction in order to distinguish the different surface active sites which are present on (and in) the Ta-MCM-41 catalyst, and the catalytic results are listed in Table 2. The high selectivity of MF and HCHO over these catalysts reveals that the redox sites are predominantly present on the surface of these catalysts at the Ta concentration below 12% wt. (equal to 15% Ta_2O_5). The essentially acid sites present

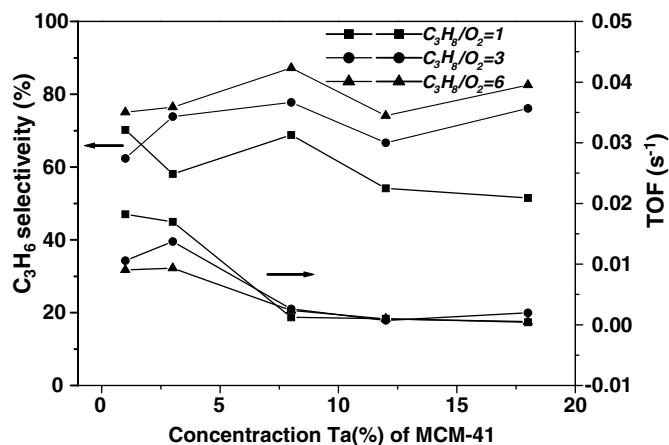


Fig. 4. The catalytic properties of propane ODH over the Ta–MCM-41 catalysts as a function of Ta concentration and C_3H_8/O_2 ratio at 500 °C with a 100 cc/min flowing rate of $C_3H_8/O_2/He$.

on the surface for the 18% Ta–MCM-41 catalyst result in the higher selectivity of DME (see Table 2) due to the presence of bulk Ta_2O_5 with acidic characteristic. The calculated turnover frequency (TOF) of the oxidation reactions over the Ta–MCM-41 catalyst is based on total Ta atom present in the catalyst since it is well-dispersed and isolated.

4. Discussions

The physical properties of the mesoporous Ta–MCM-41 catalyst as a function Ta concentration are listed in Table 3. The surface area and the pore volume of the Ta–MCM-41 catalyst dramatically decrease with increasing Ta concentration up to 12% ($Si/Ta = 20$) in MCM-41,

and the pore size of the Ta–MCM-41 catalyst only slightly decreases indicating the blockage of the pores at higher Ta concentration. The deviation from sharp and well-defined isotherm (see Fig. 1) is also observed with increasing Ta concentration in MCM-41 indicating the increase of pore size heterogeneity and the degradation of the mesoporosity at higher Ta concentration. This is consistent with the XRD results shown in Fig. 2 that the structural deformability of the Ta–MCM-41 catalyst starts at a Si/Ta ratio up to 20. The shift of the (100) peak to lower diffraction angle in the V–MCM-41 system has been reported by Sayari et al. [56] and determined that the incorporation of V atom into MCM-41 structure results in the slight increase in d-spacing. However, the results from Kevan et al. [57] and Haller et al. [58] studying in the V–MCM-41 system has revealed that the d-spacing obviously decreases with increasing vanadium concentration. The disappearance of the (210) peak at 2θ of 6° after the incorporation of vanadium into MCM-41 up to a Si/V ratio of 23 suggests that incorporation of vanadium atom to the wall of MCM-41 [57]. Thus, only the peak of (100) has been detected in the Ta–MCM-41 system with increasing Si/Ta ratio above 20 indicating the structural deformability and the presence of Ta species on the MCM-41 surface.

Raman spectra of the Ta–MCM-41 catalyst (in Fig. 3) are similar to Raman features of the Ta_2O_5/SiO_2 catalysts [42,59] with the exception of the additional Raman band at $\sim 910\text{ cm}^{-1}$ for the Ta–MCM-41 catalyst. The results indicate that the surface isolated TaO_x species (Raman band at $965\text{--}980\text{ cm}^{-1}$) are present at lower Ta concentration (below 12%), and bulk Ta_2O_5 (Raman band at $\sim 690\text{ cm}^{-1}$) is observed in the 18% Ta–MCM-41 catalyst. The new Raman band at $\sim 910\text{ cm}^{-1}$, shifting to $\sim 930\text{ cm}^{-1}$ with increasing Ta concentration, is assigned

Table 2
Catalytic properties of the Ta–MCM-41 catalysts for methanol oxidation at 300 °C

Catalysts	Conv. (%)	Activity (mmol/g h)	TOF (10^{-2} s^{-1})	Selectivity (%)			
				MF	HCHO	DME	CO_x
MCM-41	Not active						
1% Ta–MCM-41	12.7	35.8	17.9	97	2	Trace	1
3% Ta–MCM-41	15.1	49.2	8.2	82	5	9	4
8% Ta–MCM-41	20.1	48.8	3.2	73	10	10	7
12% Ta–MCM-41	9.2	23.7	1.0	70	14	16	–
18% Ta–MCM-41	10.2	27.8	0.8	52	4	42	2

Table 3
Mesoporous structural properties of the Ta–MCM-41 catalysts

Catalysts	Si/Ta (as synth.)	(ICP-AES analysis)	Surface area (m^2/g)	Pore volume (cm^3/g)	Ave. pore diameter (nm)	Wall thickness (nm)
MCM-41	–		1163	1.1	3.9	0.7
1% Ta–MCM-41	400	(1.1% Ta)	1098	1.0	3.7	0.8
3% Ta–MCM-41	100	(3.0% Ta)	1039	1.0	3.8	0.8
8% Ta–MCM-41	33	(8.1% Ta)	935	0.9	3.7	0.9
12% Ta–MCM-41	20	(11.7% Ta)	807	0.7	3.5	1.0
18% Ta–MCM-41	12	(17.6% Ta)	785	0.7	3.6	1.0

to the incorporation of Ta atom into the MCM-41 framework which is not observed in the $\text{Ta}_2\text{O}_5/\text{SiO}_2$ catalysts. The Raman intensity of this new band does not increase with increasing Ta concentration, and the shift of the band position from 910 to 930 cm^{-1} is due to the peak coupling as a shoulder peak of the Raman band at $\sim 980\text{ cm}^{-1}$. Thus, only certain amount of Ta atom can incorporate into the MCM-41 frame structure. The incorporation of Ta atom into the MCM-41 structure results in a distorted and isolated $[\text{TaO}_4]$ surrounded by the $[\text{SiO}_4]$ tetrahedrons with the presence of Ta–O–Si bridging bonds possessing the Raman bands at 830 and 475 cm^{-1} . The shift of the Raman bands from 800 to 830 cm^{-1} and 490 to 475 cm^{-1} , respectively, and the change of its relatively Raman intensity also suggest the breakage of the Si–O–Si

bonds and the cyclosiloxane rings and incorporate the Ta atom into the MCM-41 structure. The morphology of the MCM-41 and Ta–MCM-41 catalysts as a function of Ta concentration was directly monitored by SEM as shown in Fig. 5. The SEM results indicate that the MCM-41 surface starts to become rough and form nanoscale particles above 3% Ta concentration, and the nanoscale particles increases with further increasing Ta concentration up to 18%. It indicates that the presence of the Ta atom is predominately incorporated into the MCM-41 frame structure at low Ta concentration (below 3% Ta), and forms an isolate TaO_4 species on the Ta–MCM-41 surface with further increasing Ta concentration. The increase of Raman intensity at $\sim 980\text{ cm}^{-1}$ with increasing Ta concentration can determine the formation of the surface isolated TaO_4 spe-

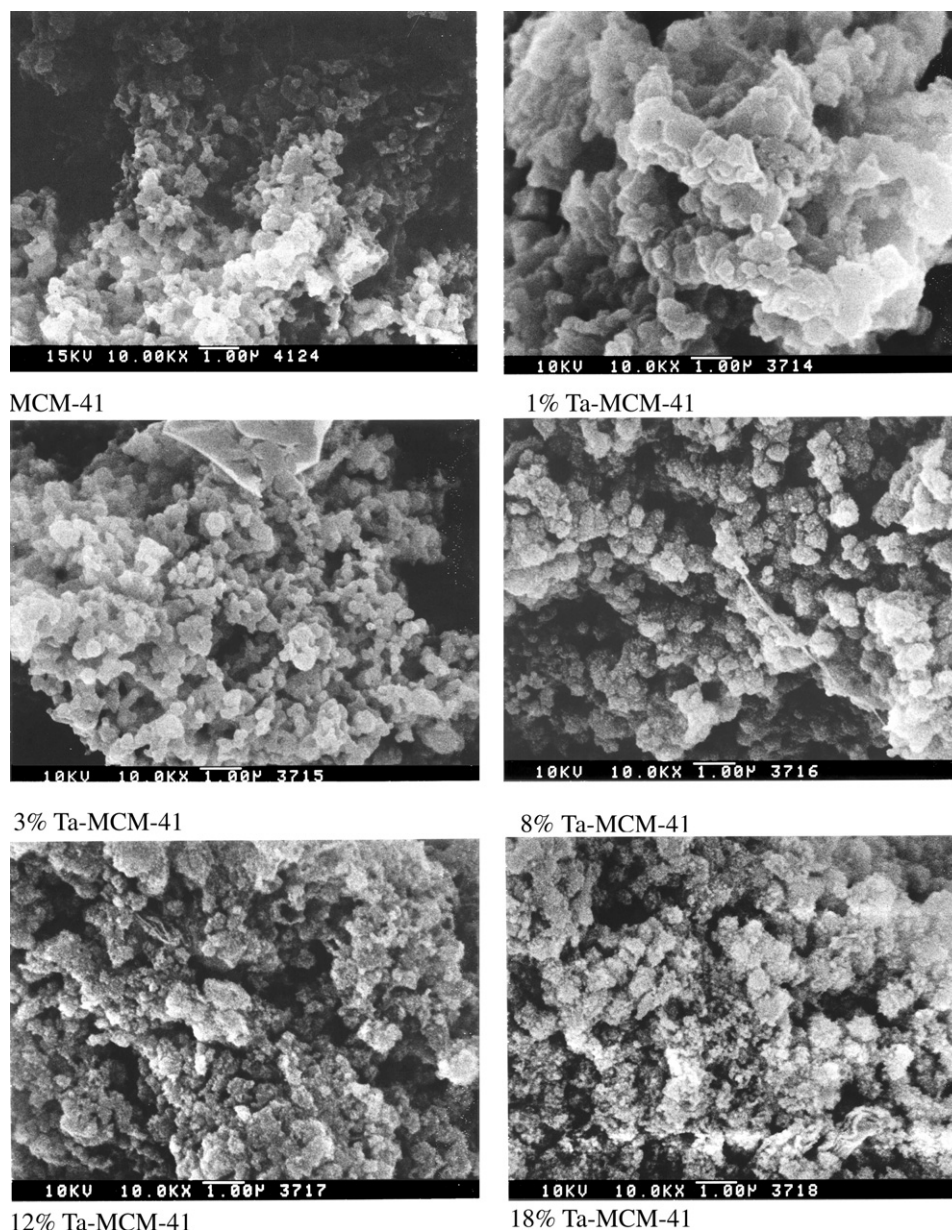


Fig. 5. SEM images of the MCM-41 and Ta–MCM-41 catalysts.

cies. The formation of the surface isolated TaO_4 species is consistent with Chen et al. [42] and Baltes et al. [59] studies on the supported tantalum oxide catalysts that the silica support possesses a lower concentration of reactive surface hydroxyls and a strong interaction with the surface TaO_x species to form an isolated TaO_4 species with one $\text{Ta}=\text{O}$ terminal bands and three $\text{Ta}-\text{O}-\text{Si}$ bridging bonds. The UV–vis–NIR DRS studies on the Ta-containing oxides and compounds have indicated that the E_g value (listed in Table 1) of the Ta–MCM-41 catalyst (above 4.5 eV) is higher than that of the $\text{Ta}_2\text{O}_5/\text{SiO}_2$ catalyst (4.4 eV). This suggests the presence of the isolated TaO_4 species which is consistent with Raman results. The polymeric and distorted TaO_6 species possess the E_g value below 4.0 eV. Thus, the addition of Ta atom into the MCM-41 forms an isolated TaO_4 species in (and on) the MCM-41 structure.

In addition, the maximum surface density to reach a monolayer coverage on silica has been determined by Chen et al., using Raman and methanol oxidation studies, to be 0.7 Ta atoms/nm² (corresponding to 5 wt% $\text{Ta}_2\text{O}_5/\text{SiO}_2$) [42]. A monolayer coverage of the surface isolated TaO_4 species on Ta–MCM-41 can be calculated, on the basis of the maximum surface density of the $\text{Ta}_2\text{O}_5/\text{SiO}_2$ catalyst, to be about 17.5% Ta_2O_5 . Raman studies on the Ta–MCM-41 catalyst (see Fig. 3) have revealed that the monolayer coverage of the isolated surface TaO_4 species on Ta–MCM-41 has been reached just below 18% Ta (equal to 22% Ta_2O_5) due to the presence of trace bulk Ta_2O_5 (Raman band at $\sim 690\text{ cm}^{-1}$) at this Ta concentration. Thus, the monolayer coverage of the isolated TaO_4 species on the Ta–MCM-41 catalysts has reached a higher value (22% Ta_2O_5) compared to the calculate value (17.5% Ta_2O_5). This is an indirect proof of the incorporation of the Ta atom into the MCM-41 frame structure. For the metals (V and Nb) in Group V, the surface VO_x and NbO_x species can be present in both V–MCM-41 and Nb–MCM-41 catalysts, and suggests that some V and Nb atoms may be incorporated within the MCM-41 framework [7,11]. The catalytic results indicate that the isolated VO_x and NbO_x species in both types of catalysts are active redox sites for methanol oxidation and similar catalytic properties due to the presence of V(or Nb)–O–Si bonds in their structure [7,11]. The surface TaO_x species on silica has found to possess redox property and bulk Ta_2O_5 possesses only acidic property [42]. Thus, three types of tantalum oxide species: an isolated TaO_4 species in the MCM-41 framework, an isolated surface TaO_4 species on the MCM-41 surface, and bulk Ta_2O_5 , are present in (and on) the Ta–MCM-41 catalysts, and their relative intensity is dependent on the Ta concentration.

Recent studies on the C_1 – C_4 hydrocarbon oxidation reactions over the supported vanadia catalysts have revealed that reaction pathways require only one surface vanadia site and that the critical rate determining step involved the bridging V–O–Support bonds [60,61]. Monolayer coverage of the supported vanadia catalysts exhibits

the high propylene selectivity, especially at low propane conversions. The deposition of surface vanadia species consumes mostly the terminal surface hydroxyls, resulting in a significant decrease in the formation of combustion products. Thus, the surface vanadia coverage and the propane/ O_2 ratio significantly affect the propylene selectivity [62]. The high oxygen concentration at a propane/ O_2 ratio of 1/10 gives rise to the highest propylene selectivity. Similar results were also obtained for the catalysts possessing lower surface vanadia coverage. It strongly suggests that propylene production is favored on highly oxidized surface vanadia species of the supported vanadia catalysts where the surface V^{5+} population is over 90% [62], and reduced surface $\text{V}^{4+}/\text{V}^{3+}$ sites favor CO^* formation via an oxygenated intermediate [62]. In addition, catalytic reactivity (as measured by turnover frequency; TOF) is independent of the surface density of the two-dimensional vanadia overlayer on the oxide support and both polymerized and isolated surface vanadium species are active sites for propane oxidation.

The catalytic properties of propane ODH over the Ta–MCM-41 catalysts indicate that the high propylene selectivity is favored at higher $\text{C}_3\text{H}_8/\text{O}_2$ ratio of 6:1, and the increase of Ta concentration has no significant effect on the propylene selectivity since only one active site required for the reaction. In addition, the high reactivity of propane ODH over the Ta–MCM-41 catalyst is favored at lower $\text{C}_3\text{H}_8/\text{O}_2$ ratio of 1:1, and decrease with increasing Ta concentration (see Fig. 4). From the combination of the structural characterization and the propane ODH, the incorporation of Ta atom into MCM-41 structure to form Ta–O–Si bonds at lower Ta concentration is responsible for the high reactivity of propane ODH.

The catalytic properties of the Ta–MCM-41 catalysts were further probed with the sensitive methanol oxidation reaction in order to distinguish the different surface active sites which are present on (and in) the Ta–MCM-41 catalyst, and the catalytic results are listed in Table 2. The high selectivity of MF and HCHO over these catalysts has revealed that the redox sites are predominantly present on the surface of these catalysts at the Ta concentration below 12% Ta (equal to 15% Ta_2O_5). The essentially acid sites present on the surface for the 18% Ta–MCM-41 catalyst result in a higher selectivity of DME (see Table 2) due to the presence of bulk Ta_2O_5 with acidic property. It is similar to Chen et al.'s [42] studies on the $\text{Ta}_2\text{O}_5/\text{SiO}_2$ catalysts possessing a high redox property. The reactivity of methanol oxidation over the Ta–MCM-41 catalyst decreases with increasing Ta concentration (see Table 2) which is similar to the catalytic results of propane ODH (Fig. 4). From the previous structural characterization, three types of tantalum oxide species: an isolated TaO_4 species in the MCM-41 framework, an isolated surface TaO_4 species on the MCM-41 surface, and bulk Ta_2O_5 , are found in (and on) the Ta–MCM-41 catalysts. The incorporation of Ta atom into MCM-41 structure to form Ta–O–Si bonds in MCM-41 framework results in a higher activity,

and the presence of the surface TaO₄ species on the catalyst possessing a lower activity results in the decrease of methanol reactivity with increasing Ta concentration. Thus, the local structure of the metal atoms in the M–MCM-41 (M = V, Nb, and Ta) forms an isolated active site with similar bridging M–O–Si bonds on the surface and in the frame structure of MCM-41. The well-dispersed isolated surface active sites exhibit high redox catalytic properties and the bridging M–O–Si bonds are the critical functionalities for its catalytic applications.

5. Conclusions

The Ta–MCM-41 catalysts possess a mesoporous structure, and the surface area and the pore volume of the Ta–MCM-41 catalyst dramatically decrease with increasing Ta concentration up to 12% Ta due to the blockage of the pores and the structural deformability of the Ta–MCM-41 catalyst at higher Ta concentration. Raman results indicate that the incorporation of Ta atom into the MCM-41 structure forms a distorted and isolated [TaO₄] surrounded by the [SiO₄] tetrahedrons with the presence of Ta–O–Si bridging bonds, and three types of tantalum oxide species: an isolated TaO₄ species in the MCM-41 framework, an isolated surface TaO₄ species on the MCM-41 surface, and bulk Ta₂O₅, can be present individually or coexist on the Ta–MCM-41 catalysts, and its relatively intensity is dependent on the Ta concentration. The propane ODH and methanol oxidation reactions have indicated that the Ta–MCM-41 catalysts possesses a high redox property to produce propylene and MF. The local structure of the Ta atoms in the Ta–MCM-41 forms an isolated active site with the bridging Ta–O–Si bonds on the surface and in the frame structure of MCM-41. The well-dispersed isolated surface active sites exhibit high redox catalytic properties and the bridging Ta–O–Si bonds are responsible for its catalytic applications.

Acknowledgments

The financial support of the National Science Council of Taiwan (Grant No. NSC 92-2214-E-005-004) and partially support from the Green Chemistry-Products group sponsored by the Ministry of Education are gratefully acknowledged. We thank the Center of Expansive Instruments at National Chung Hsing University for SEM studies and the Department of Material Engineering at National Chung Hsing University for XRD studies.

References

- [1] J.S. Beck, C.T.W. Chu, I.D. Johnson, C.T. Kresge, M.E. Leonowicz, W.J. Roth, J.C. Vartuli, US Patent 5, 098, 1992, p. 684.
- [2] G. Du, S. Lim, Y. Yang, C. Wang, L. Pfefferle, G.L. Haller, *Appl. Catal. A: Gen.* 302 (2006) 48.
- [3] V. Parvulescu, C. Anastasescu, C. Constantin, B.L. Su, *Catal. Today* 78 (2003) 477.
- [4] Q. Zhang, Y. Wang, Y. Ohishi, T. Shishido, Katsuomi Takehira, *J. Catal.* 202 (2001) 308.

- [5] D. Wei, H. Wang, X. Feng, W.-T. Chueh, P. Ravikovitch, M. Lyubovskiy, C. Li, T. Takeguchi, G.L. Haller, *J. Phys. Chem. B* 103 (1999) 2113.
- [6] M. Chatterjee, T. Iwasaki, H. Hayashi, Y. Onodera, T. Ebina, T. Nagase, *Chem. Mater.* 11 (1999) 1368.
- [7] C.B. Wang, G. Deo, I.E. Wachs, *J. Catal.* 178 (1998) 640.
- [8] K.J. Chao, C.N. Wu, H. Chang, L.J. Lee, S. Hu, *J. Phys. Chem. B* 101 (1997) 6341.
- [9] S. Vetrivel, A. Pandurangan, *Catal. Lett.* 99 (3–4) (2005) 141.
- [10] M. Ziolek, A. Lewandowska, B. Grzybowska, *React. Kinet. Catal. Lett.* 80 (2) (2003) 199.
- [11] X. Gao, I.E. Wachs, M. Wong, Jackie Ying, *J. Catal.* 203 (2001) 18.
- [12] J. Ying, C.P. Mehnert, M.S. Wong, *Angew. Chem., Int. Ed.* 38 (1999) 56.
- [13] B. Yuliarto, I. Honma, Y. Katsumura, H. Zhou, *Sensors Actuat. B* 114 (2006) 109.
- [14] J.-Y. Piquemai, E. Briot, G. Chottard, P. Tougne, J.-M. Manoli, J.-M. Bregeault, *Micropor. Mesopor. Mater.* 58 (2003) 279.
- [15] Z. Zhang, J. Suo, X. Zhang, S. Li, *Appl. Catal. A: Gen.* 179 (1999) 11.
- [16] S. Higashimoto, Y. Hu, R. Tsumura, K. Iino, M. Matsuoka, H. Yamashita, Y.G. Shul, M. Che, M. Anpo, *J. Catal.* 235 (2005) 272.
- [17] R.K. Rana, B. Viswanathan, *Catal. Lett.* 52 (1998) 25.
- [18] M. Selvaraj, T.G. Lee, *Micropor. Mesopor. Mater.* 85 (2005) 39.
- [19] S. Samanta, N.K. Mai, A. Bhaumik, *J. Mol. Catal. A: Chem.* 236 (2005) 7.
- [20] Y. Ohishi, T. Kawabata, T. Shishido, K. Takaki, Q. Zhang, Y. Wang, K. Takehira, *J. Mol. Catal. A: Chem.* 230 (2005) 49.
- [21] Y. Li, X. He, S. Wu, K. Zhang, G. Zhou, J. Liu, K. Zhen, T. Wu, T. Cheng, *J. Nat. Gas Chem.* 14 (2005) 207.
- [22] Z. Zhu, Z. Zhang, L. Kevan, *J. Phys. Chem. B* 103 (1999) 2680.
- [23] N. Igarashi, S. Kidani, R. Ahemaito, K. Hashimoto, T. Tatsumi, *Micropor. Mesopor. Mater.* 81 (2005) 97.
- [24] Y. Kong, X. Guo, F. Zhang, S. Jiang, J. Wang, Y. Lu, Q. Yan, *Mater. Lett.* 59 (2005) 3099.
- [25] N. Thanabodeekij, W. Tanglumlert, E. Gulari, S. Wongkasemjit, *Appl. Organometal. Chem.* 19 (2005) 1047.
- [26] M.L. Ocelli, S. Biz, A. Auroux, *Appl. Catal. A: Gen.* 183 (1999) 231.
- [27] J.M.R. Gallo, I.S. Paulino, U. Schuchardt, *Appl. Catal. A: Gen.* 266 (2004) 223.
- [28] S. Biz, M.L. Ocelli, *Catal. Rev. Sci. Eng.* 40 (1998) 329.
- [29] A. Corma, *Chem. Rev.* 97 (1997) 2373.
- [30] G. Bellussi, G. Centi, S. Perathoner, F. Trifiro, *ACS Symp. Ser.* 523 (1996) 281.
- [31] S. Takenaka, T. Kuriyama, T. Tanaka, T. Funabiki, S. Yoshida, *J. Catal.* 155 (1995) 196.
- [32] M.M. Koranne, J.G. Goodwin Jr., G. Marcelin, *J. Catal.* 148 (1994) 388.
- [33] L. Owen, H.H. Kung, *J. Catal.* 144 (1993) 202.
- [34] F. Arena, F. Frusteri, A. Parmaliana, N. Giordano, *J. Catal.* 143 (1993) 299.
- [35] S.T. Oyama, A.M. Middlebrook, G.A. Sormorjai, *J. Phys. Chem.* 94 (1990) 5029.
- [36] G. Deo, I.E. Wachs, *J. Haber, Crit. Rev. Surf. Chem.* 4 (1994) 141.
- [37] I.E. Wachs, B.M. Weckhuysen, *Appl. Catal. A: Gen.* 157 (1997) 67.
- [38] I.E. Wachs, in: J.J. Spivey (Ed.), *Catalysis*, vol. 13, The Royal Society of Chemistry, Cambridge, 1977, p. 37.
- [39] N. Das, H. Eckert, H. Hu, I.e. Wachs, J.F. Walzer, F.J. Feher, *J. Phys. Chem.* 97 (1993) 8240.
- [40] G.T. Went, S.T. Oyama, A.T. Bell, *J. Phys. Chem.* 94 (1990) 4240.
- [41] X. Gao, S.R. Bare, B.M. Weckhuysen, I.E. Wachs, *J. Phys. Chem. B* 102 (1998) 10842.
- [42] Y. Chen, J.L.G. Fierro, T. Tanaka, I.E. Wachs, *J. Phys. Chem. B* 107 (2003) 5243.
- [43] X. Gao, J.M. Jehng, I.E. Wachs, *J. Catal.* 209 (2002) 325.
- [44] B.M. Weckhuysen, R.A. Schoonheydt, *Catal. Today* 49 (1999) 441.
- [45] J.J. Venter, M.A. Vannice, *Appl. Spectrosc.* 42 (1988) 1096.
- [46] W.N. Delgass, G.L. Haller, R. Kellerman, J.H. Lunsford, *Spectroscopy in Heterogeneous Catalysis*, Academic Press, New York, 1979.

- [47] E.A. Davis, N.F. Mott, *Philos. Mag.* 22 (1970) 903.
- [48] A.A. Hossain, C.A. Hogarth, J. Bynon, *J. Mater. Sci. Lett.* 13 (1994) 1144.
- [49] G.A. Khan, C.A. Hogarth, *J. Mater. Sci. Lett.* 26 (1991) 412.
- [50] A. Miecznikowski, J. Hanuza, *Zeolites* 7 (1987) 249.
- [51] C.J. Brinker, R.J. Kirkpatrick, D.R. Tallant, B.C. Bunker, B. Montez, *J. Non-Cryst. Solids* 99 (1988) 418.
- [52] B.A. Morrow, A.J. McFarlan, *J. Non-Cryst. Solids* 120 (1990) 61.
- [53] I.E. Wachs, J.M. Jehng, G. Deo, B.M. Weckhuysen, V.V. Gulians, J.B. Benziger, *Catal. Today* 32 (1996) 47.
- [54] D.C. Sun, S. Senz, D. Hesse, *J. Eur. Ceram. Soc.* 24 (2004) 2453.
- [55] C. Tealdi, M.S. Ialam, L. Malavasi, G. Flor, *J. Solid State Chem.* 177 (2004) 4359.
- [56] K.M. Reddy, I. Moudrakovski, A. Sayari, *J. Chem. Soc. Chem. Commun.* (1994) 1059.
- [57] Z. Luan, J. Xu, H. He, J. Klinowski, L. Kevan, *J. Phys. Chem.* 100 (1996) 19595.
- [58] D. Wei, H. Wang, X. Feng, W. Chueh, P. Ravikovitch, M. Lyubovsky, T. Takehuchi, G.I. Haller, *J. Phys. Chem.* 103 (1999) 2113.
- [59] M. Baltes, A. Kytokivi, B.M. Weckhuysen, R.A. Schoonheydt, P. Van Der Voort, E.F. Vansant, *J. Phys. Chem. B* 105 (2001) 6211.
- [60] I.E. Wachs, B.M. Weckhuysen, *Appl. Catal. A: Gen.* 157 (1997) 67.
- [61] X. Gao, J.M. Jehng, I.E. Wachs, *J. Catal.* 209 (2002) 325.
- [62] M.M. Bettahar, G. Costentin, G. Savary, J.C. Lavalley, *Appl. Catal. A* 145 (1996) 1.